Seven Sisters: a mission to study fundamental plasma physical processes in the solar wind and a pathfinder to advance space weather prediction

Katariina Nykyri[1]*, Xuanye Ma[1], Brandon Burkholder[2], Yu-Lun Liou[1], Roberto Cuéllar[1], Shiva Kavosi[1], Joseph E. Borovsky[3], Jeff Parker[4], Mitchell Rosen[4], Lauren De Moudt[4], Robert Wilkes Ebert[5], Keiichi Ogasawara[5], Merav Opher[6], David Gary Sibeck[7], Simone Di Matteo[7,8], Nicholeen Viall[7], Samantha Wallace[7], Therese M. Jorgensen[9], Michael Hesse[9], Matthew J. West[10], Laxman Adhikari[11], Matthew R. Argall[12], Jan Egedal[13], Frederick Wilder[14], Jeffrey Broll[15], Gangkai Poh[8], Simon Wing[16] and Christopher Russell[17]

[1]Department of Physical Sciences and Center for Space and Atmospheric Research, Embry-Riddle Aeronautical University, Daytona Beach, FL, United States, [2]UMBC Goddard Planetary Heliophysics Institute, Baltimore, MD, United States, [3]Space Science Institute, Boulder, CO, United States, [4]Advanced Space LLC, Westminster, CO, United States, [5]Southwest Research Institute, San Antonio, TX, United States, [6]Department of Astronomy, Boston University, Boston, MA, United States, [7]NASA Goddard Space Flight Center, Greenbelt, MD, United States, [8]Catholic University of America, Washington, DC, United States, [9]NASA Ames Research Center, Moffett Field, CA, United States, [10]Southwest Research Institute, Boulder, CO, United States, [11]The Center for Space Plasma and Aeronomic Research, The University of Alabama in Huntsville, Huntsville, AL, United States, [12]Space Science Center, The University of New Hampshire, Durham, NH, United States, [13]Department of Physics, The University of Wisconsin Madison, Madison, WI, United States, [14]Department of Physics, The University of Texas, Arlington, TX, United States, [15]Los Alamos National Laboratory, Los Alamos, NM, United States, [16]John Hopkins University, Applied Physics Laboratory, Laurel, MD, United States, [17]Department of Earth, Planetary and Space Sciences, University of California, Los Angeles, Los Angeles, CA, United States

This paper summarizes the Seven Sisters solar wind mission concept and the outstanding science questions motivating the mission science objectives. The Seven Sisters mission includes seven individual spacecraft designed to uncover fundamental physical processes in the solar wind and provides up to ≈ 2 days of advanced space weather warnings for 550 Earth days during the mission. The mission will collect critical measurements of the thermal and suprathermal plasma and magnetic fields, utilizing, for the first time, Venus—Sun Lagrange points. The multi-spacecraft configuration makes it possible to distinguish between spatial and temporal changes, define gradients, and quantify cross-scale transport in solar wind structures. Seven Sisters will determine the 3-D structure of the solar wind and its transient phenomena and their evolution in the inner heliosphere. Data from the Seven Sisters mission will allow the identification of physical processes and the quantification of the relative contribution of different mechanisms responsible for suprathermal particle energization in the solar wind.

1 Introduction

This paper presents the Seven Sisters inner heliospheric mission concept, consisting of seven identical spacecraft that will occupy, for the first time, Venus–Sun Lagrange (VL) points to determine the 3-D structure of the solar wind and its transient phenomena and their evolution in the inner heliosphere. The mission will also identify and quantify the critical physical processes energizing and transporting particles in the solar wind.

This effort originally started in 2016, when PI's (Nykyri) home institution (ERAU), by the initiative of the interim president, Dr. Karen Holbrook, was computing ideas for the "Accelerate Research Initiative (ARI)". Nykyri's group had just published a method to construct a technique to identify the k vector, phase, and amplitude of 200–2,000 km wavelength kinetic magnetosonic waves within 36,000 km wavelength Kelvin–Helmholtz waves and demonstrated plasma heating by these waves from the shocked solar wind into the Earth's magnetosphere (Moore et al., 2016). Inspired by these results, Nykyri proposed an ARI project to develop a solar wind mission concept with appropriate spacecraft separations such that the solar wind properties, structure, and magnetohydrodynamic (MHD) wave spectrum (with k vector, phase, and amplitude) in the solar wind could be accurately constructed, which would allow advanced prediction of the space weather and the interplanetary magnetic field (IMF) B_z component. Nykyri was awarded this internal grant for 140,000 USD and was able to hire, support, and partially support more people in her team (Dr. Ma, Dr. Burkholder, and ERAU students) to work on mission concept science and engineering. The initial engineering work resulted in two ERAU M.S. theses, one in engineering physics (Herring (2019)) and one in aerospace engineering (Rangel (2020)), with stage-1 of the high-resolution solar wind model (not yet published) and produced a multi-spacecraft interpolation technique for solar wind structure determination (Burkholder et al., 2020a).

In 2021, NASA solicited proposals for the Heliophysics Mission Concept Studies, at which point Nykyri invited other people to join the team who had relevant science, multi-spacecraft mission, and instrumentation experience. NASA received 14 proposals, of which six were funded for future concept studies. Unfortunately Seven Sisters was not one of them, and at this point, there was no ARI funding left. Luckily, during past several years, Nykyri had accumulated and saved most of her indirect return research funds and was able to contract Advanced Space to perform the mission orbital mechanics and part of the engineering analysis to address the feasibility of the mission based on expected masses of the instruments. The instrument information was provided by instrument leads at SwRI and UNH. In the summer of 2022, Nykyri reached out to the broader heliophysics community with expertise on mission objectives, including several early career scientists. The mission engineering and costing analysis was completed in August 2022, and the mission team submitted two white papers to the Decadal Survey in August 2022, one focusing on the science motivating the mission (Nykyri et al. (2022a)) and the other on mission engineering (Nykyri et al. (2022b)).

A multi-spacecraft solar wind mission is not a new concept. NASA's Sentinels mission (NASA (2006)) was proposed and studied by the Living With a Star Sentinels Science and Technology Definition Team in 2006 and was intended to be a "multi-spacecraft mission comprising of 1) a constellation of four identically instrumented Inner Heliospheric Sentinels to make *in situ* measurements of the plasma, energetic particle, and fields environment as close to the Sun as 0.25 AU as well as multi-point remote-sensing observations of solar X-ray, radio, gamma-ray, and neutron emissions; 2) a Near-Earth Sentinel in Sun-synchronous orbit for ultraviolet and white-light observations of the corona; and 3) a Far Side Sentinel in heliocentric orbit at 1 AU to measure the photospheric magnetic field from positions 60°–120° ahead of the Earth." The Sentinels mission science goals were to "study 1) the acceleration and transport of solar energetic particles (SEPs) and 2) the initiation and evolution of coronal mass ejections (CMEs) and interplanetary shocks in the inner heliosphere." It was also planned that during the 3-year nominal mission, Sentinels observations would be supplemented by observations both from other spacecraft, such as the Solar Terrestrial Relations Observatories (STEREO) and the Solar Dynamics Observatory (SDO).

Currently, the single spacecraft Parker Solar Probe (launched in 2018) and Solar Orbiter (launched in 2020) can be considered "inner Sentinels" and the coordination with other missions from Heliophysics fleet (e.g., Wind, Artemis, and MMS), closer to Earth, provide measurements of the solar wind at a larger scale. Recently, NASA selected the nine-spacecraft MidEx-line HelioSwarm mission to be launched in 2028 with a main goal of studying plasma turbulence in the solar wind.

Going forward, we need dedicated multi-spacecraft solar wind missions with cross-calibrated instruments to study the complex structure and dynamics of the inner heliosphere. Seven Sisters (see **Figure 1**) will be the first mission to occupy the Venus–Sun Lagrange points, enabling up to 1–2 days of advanced *in situ* measurements of the solar wind before it reaches the Earth.

2 Scientific motivation for the Seven Sisters mission

In this section, we motivate the Seven Sisters mission and briefly describe the compelling, unknown science questions and measuring requirements. These science questions are used to formulate the targeted mission science objectives in **Section 3.1**.

The solar wind (SW) is the highly structured, multi-scale, and collision-less plasma (Marsch and Goldstein, 1983; Borovsky, 2008). More research studies have been carried out for understanding the origin of the fast and slow SW, as well as the nature of turbulence
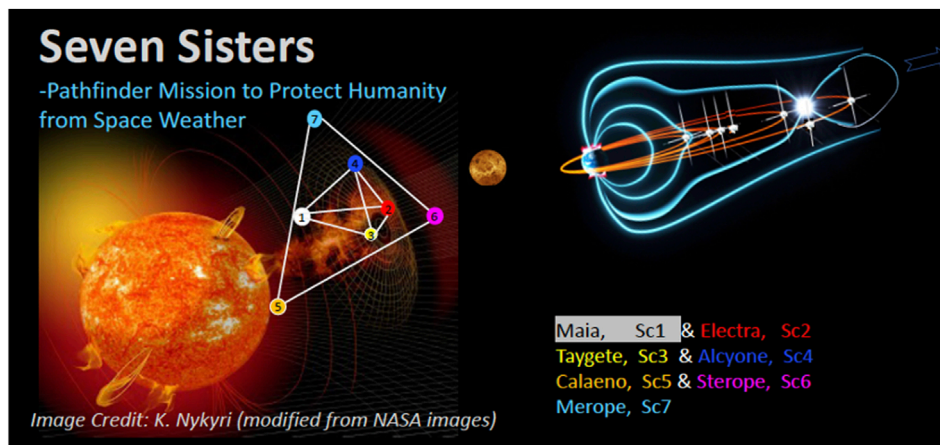
FIGURE 1
Artistic visualization of the Seven Sisters constellation during its first mission phase. The name is derived from Greek mythology. The spacecraft names together with color codes, which is designed to be inclusive of people with color identification deficiency, are shown in the figure.

in the SW in the energy containing, inertial, and dissipation ranges (Belcher and Davis Jr., 1971; Sheeley et al., 1976; Goldstein et al., 1994; Leamon et al., 1998; Bale et al., 2005; Adhikari et al., 2015; Abbo et al., 2016; Zank et al., 2017; 2018; Adhikari et al., 2020). The large- (0.6 AU to 1 AU) and intermediate-scale (1.5–100 Mm) structure and processes of the SW, such as interplanetary shocks, coronal mass ejections, heliospheric current sheet (HCS) dynamics, stream and co-rotating interaction regions (SIRs/CIRs), solar wind flux tubes (SWFTs), and magnetohydrodynamic waves have an impact on particle energization and propagation, as well as on the interplanetary magnetic field orientation on Earth and thus on the evolution of magnetospheric processes. However, their evolution in the inner heliosphere has not been adequately investigated yet, due to the lack of simultaneous, coordinated, multi-point, multi-scale, *in situ* observations at appropriate spacecraft (SC) separations.
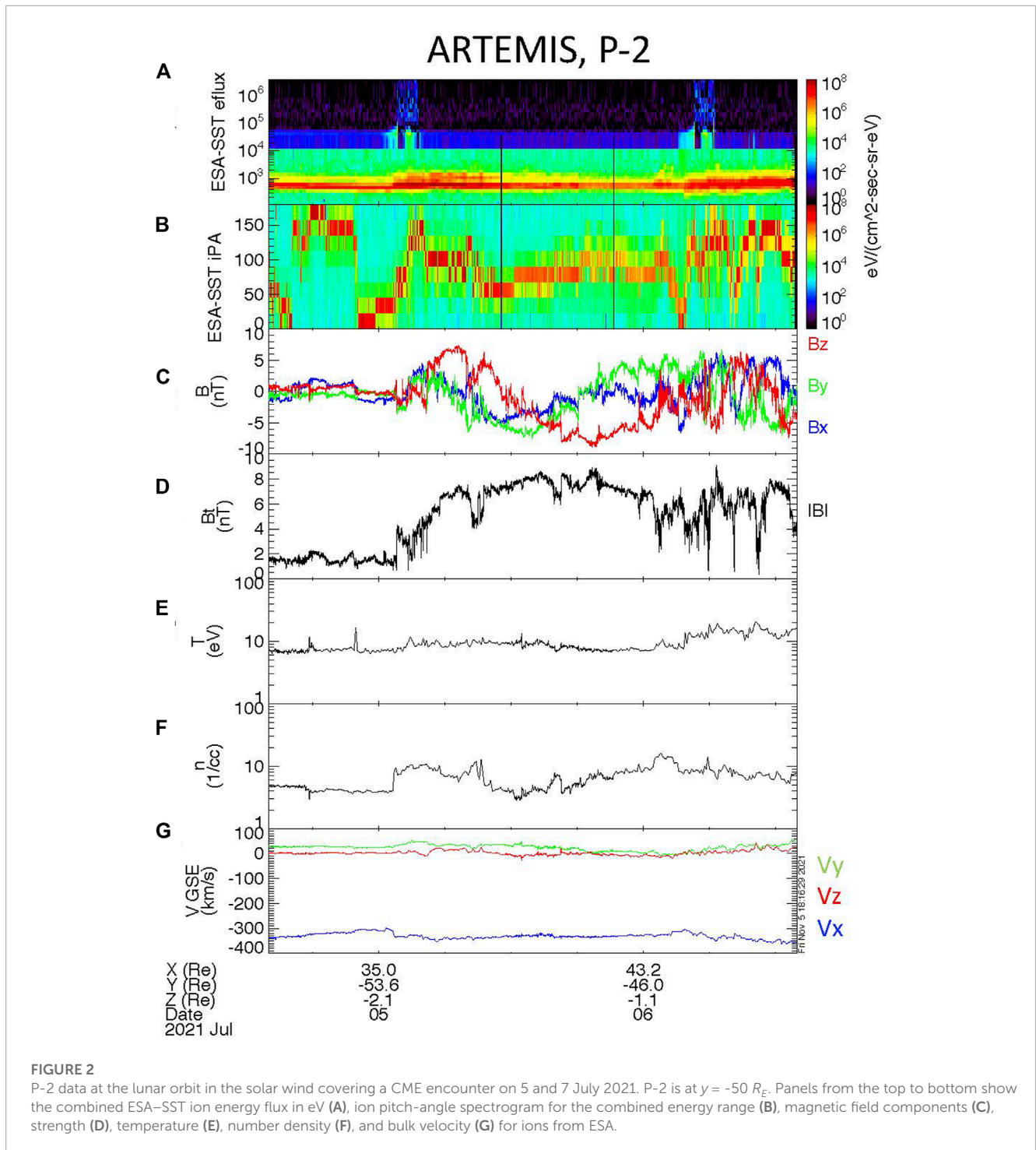
As it takes the SW $\approx 1\,h$ at its typical speed to reach the Earth from the Earth–Sun L1 point (EL1), the EL1 measurements cannot provide sufficient warning time for space weather operations. Furthermore, if the structure is present in the SW (Burkholder et al., 2020a), single SC measurements at EL1 will lead to inaccuracies when forecasting or developing various space weather warnings, e.g., for radiation belt electron flux enhancements or the Kp-index (Sexton, Ernest Scott et al., 2019). Missing this structure would also lead to wrong conclusions when interpreting the onset conditions of the physical processes at the magnetopause (Nykyri et al., 2019; Burkholder et al., 2020b) and in statistical magnetosheath and magnetospheric studies (Dimmock et al., 2013; Ma et al., 2020) that use lagged observations from a single monitor at EL1 for characterizing the SW properties and IMF orientation at the bow-shock nose.

Next, we briefly discuss the various solar wind transients, major science questions associated with them, and the new measurements required to make progress in addressing these science questions.

2.1 SW structures and required new measurements

2.1.1 Coronal mass ejections and the CME sheath/ejecta interface

Growing in size from less than a solar radius ($R_\odot$) to approximately $50R_\odot$ ($\approx 35\,Gm$) at 1 AU, CMEs are important for energetic particle dynamics and acceleration (Joyce, C. J. et al., 2021). When the CME propagates faster than the ambient SW, a shock wave develops in front of it. White-light coronagraph and energetic ($E > 4$ MeV) proton data have revealed that large solar energetic particle events and their intensities are highly correlated with the CME occurrence and with the size and speed of CMEs (Kahler et al., 1984). Theoretical models also support particle acceleration at CME driven shocks (Zank et al., 2000). Recently, a conjoined observation between the Parker Solar Probe at 0.32 AU and STEREO A at 1 AU indicated significant transport processes acting on SEPs during the 0.7 AU distance despite the fact that the large-scale CME appeared similar (Joyce, C. J. et al., 2021). These SC positions, while radially aligned along the CME direction (based on the ENLIL + Cone model), were not azimuthally aligned along the same IMF field lines, which may further contribute to the differences in SEP properties, assuming that strongly field-aligned particles easily escape when some physical processes (e.g., reconnection (Fermo et al., 2014) or Kelvin–Helmholtz instability (KHI) (Foullon et al., 2011; 2013; Nykyri and Foullon, 2013; Páez et al., 2017)) within CME or CME boundary change the magnetic topology. **Figure 2** shows an example of ARTEMIS (P-2) observations of an interplanetary CME on 7/5/2021–07/06/2021. The spacecraft crossing into the CME is characterized by a compressed magnetic field (d) and density (f). The combined ESA-SST ion pitch-angle (PA) distributions (b) show a lot of variability at the boundaries of the CME. Trapped, more stable, and closer to $\approx 90°$ PA populations (roughly bounded by the black vertical lines in panel (b)) coincide with B_z, turning negative, and a region of negative B_z (red trace) within the CME (c), which is characterized by

FIGURE 2
P-2 data at the lunar orbit in the solar wind covering a CME encounter on 5 and 7 July 2021. P-2 is at $y = -50\ R_E$. Panels from the top to bottom show the combined ESA–SST ion energy flux in eV **(A)**, ion pitch-angle spectrogram for the combined energy range **(B)**, magnetic field components **(C)**, strength **(D)**, temperature **(E)**, number density **(F)**, and bulk velocity **(G)** for ions from ESA.

higher magnetic field strength (d) and reduced plasma density when compared to the compressed plasma at the boundary of the CME (f). Both parallel and anti-parallel particle fluxes exist at the boundary layer of the CME, such that parallel fluxes change to anti-parallel when the B_x component changes from negative to positive (or *vice versa*). Enhanced fluxes of energetic particles (a) (up to 1 MeV) are observed to propagate mostly anti-parallel to the magnetic field at the edges of the CME. As the 100 s of keV to 1 MeV particles are not present at the center of the observed CME transition, it may indicate

they are locally accelerated by boundary layer processes or the spacecraft trajectory does not cross into the region where the trapped high-energy core is present. The plasma flow velocity (g) associated with this CME is modest, and no large velocity gradient exists when moving from the ambient SW to the CME. To assess the particle acceleration, magnetic field topology and transport processes within CME require multi-point, volumetric measurements.

CME sheaths drive intense geospace storms and can also affect the radiation on Earth, and other planets (Kilpua et al., 2017;

2021). Similar to the Earth's magnetospheric boundary, the velocity shear-driven KHI can grow at the CME sheath-ejecta interface (Foullon et al., 2011; 2013; Nykyri and Foullon, 2013), which may result in rich turbulence and intermittent structures, e.g., magnetic islands with a radius comparable to one-third of the KH wavelength created by magnetic reconnection (Nykyri and Otto, 2001). After the KHI saturates, it creates a thicker sheath region around CME. Subsequently, as the fastest growing wavelength is comparable to $(2-4)\pi\Delta$ (Miura and Pritchett, 1982), where Δ is the velocity shear layer thickness, any subsequent KH growth at the ejecta interface of expanding CME between the low corona and Earth requires a longer wavelength. At the Earth's magnetopause, multi-SC observations have verified that the KHI can trigger magnetic reconnection (Nykyri et al., 2006; Eriksson et al., 2016), and more recently, MMS data have revealed that both the KH- and drift mirror instability (DMI) result in energetic electron (30 keV–600 keV) loss into the magnetosheath (MSH) or deeper into the magnetosphere (MSP) (Kavosi et al., 2018; Nykyri et al., 2021a). It has also been shown how ions (Moore et al., 2017; Moore and Nykyri, 2017; Nykyri et al., 2021b) and electrons (Nykyri et al., 2021b) can be effectively heated by ion and sub-ion scale waves (Wilder et al., 2016; 2020) driven by the KHI. As the magnetic tension force can stabilize the KHI, at the Earth's MSP, the KHI is more often observed downstream of the quasi-parallel shock when compared to the quasi-perpendicular shock (Henry et al., 2017). By the same analog, the KHI growth is likely asymmetric due to the different magnetic fields at the different flanks of the CME (Nykyri, 2013; Nykyri and Foullon, 2013). This can lead to asymmetry in its drag properties (Kay et al., 2015) and may turn the CME away from its original direction (Nykyri and Foullon, 2013). Furthermore, similar to the Earth's MSP, the KHI driven perturbations, reconnection, and subsequent magnetic topology changes may affect energetic particle dynamics and escape from CMEs (Sorathia et al., 2017; Sorathia et al., 2019; Nykyri et al., 2021b).

For the space weather forecast, central science questions (SQs) are as follows:

SQ 1.1 How do CMEs radially evolve during propagation and azimuthal expansion in interplanetary space? What is their multi-scale magnetic structure and topology, as measured simultaneously at flank regions, in central CME and at the leading edge?

SQ 1.2 What are the drag properties of the CME sheath region? How are they related to local magnetic field topology? Under what conditions the viscous processes (at the CME-ejecta sheath boundary), such as the KHI, are able to change the direction of the CME, if they form asymmetrically (due to different magnetic tension forces (Nykyri and Foullon, 2013)) at different flanks of the CME?

SQ 1.3 What are the physical mechanisms that generate fluctuations at CME sheath regions and drive eddy viscosity leading to drag forces? Can the KHI that has been observed at the CME-ejecta sheath boundary in the low corona re-grow after saturation with a larger wavelength? Like in the Earth's magnetopause, does KHI drive secondary processes, i.e., reconnection, ion and electron scale waves, and turbulence at CME sheath regions?

SQ 1.4 Which physical processes are responsible for particle acceleration and transport within CME and its substructure? How do CME sheath region processes affect plasma heating, transport, and dynamics of energetic particles?

To solve these SQs, a large azimuthal coverage of *in situ* observations with at least two-point measurements (i.e., radial line measurement) is desired. Such a measurement will largely help in validating and improving the current numerical CME modeling and will sequentially improve the capability of space weather prediction. Ideally, an inner heliospheric observatory with a combination of azimuthally separated multi-point, radial, and multi-scale volumetric (each spacecraft constellation forms two nested tetrahedrons at scales from 1,000 km to 15,000 km and from 15,000 km to 100,000 km) *in situ* and remote-sensing measurements will be developed during next decades and beyond. At the very minimum, *in situ* measurements of magnetic fields and thermal and suprathermal plasma are required. Remote sensing measurements of the EUV spectrum or total electron content between spacecraft would be highly desired.

To determine the evolution of the KHI and resulting secondary processes at the CME boundary requires measurements of magnetic fields, thermal plasma, and suprathermal fluxes and pitch-angle distributions at a minimum of two longitudinally separated points from 1.5 Mm to >50 Mm along the KH **k** vector. As the probability of measuring this narrow layer is small, several azimuthally separate longitudinal measurements of the magnetic field and thermal and suprathermal plasma is required.

The Seven Sisters mission will enable addressing these science questions with unprecedented capability via evolving multi-spacecraft, multi-scale configurations during different mission phases (see Section 2.2): throughout the duration of the planned 7-year mission, we expect to have over 2,000 CME encounters with simultaneous two-spacecraft line measurements at VL4, VL1, and VL5; 450 encounters with four to seven spacecraft volumetric measurements; and over 8,000 encounters with a single spacecraft.

2.1.2 Heliospheric current sheet

The HCS separates regions of opposite magnetic polarity and is the largest coherent structure within the heliosphere (Riley et al., 2002). Early statistical studies using spacecraft data at 1 AU have estimated the thickness of the HCS to be approximately 10,000 km, while a surrounding plasma sheet is thicker by a factor of 30 (Winterhalter et al., 1994; Smith, 2001). The HCS forms a highly variable wavy structure in the heliosphere due to the angle between the Sun's rotational axis and Sun's magnetic dipole axis due to the variable and dynamic quadrupolar magnetic field. The large-scale, large-amplitude oscillations of the HCS current sheet would result in large-scale compressions and rarefications of the magnetic field in the inner heliosphere. Therefore, it is expected that the HCS and its dynamics are important for modulating fluxes of energetic particles that enter the inner heliosphere. It has been shown that the HCS can cause fast drifts along it and act as a major source of cosmic rays in the heliosphere (Jokipii and Levy, 1977).

It has also been proposed that the kinks in the HCS may alternatively be attributed to a network of extended current sheets from multiple helmet streamers (Crooker et al., 1993). In addition, magnetic reconnection can be responsible for some of the structures in the heliospheric plasma sheet and HCS (Crooker et al., 2004; Kepko et al., 2016).

Despite 60+ years of space age, there has not been a dedicated mission to measure the intermediate- and large-scale structure of the

HCS and associated physical processes. Several outstanding science questions still exist:

SQ 2.1 What creates the structure in the HCS? Can there be eigenmodes in the HCS oscillations? If they are present, what are the frequencies, wavelengths, and how are they dependent on solar wind properties? How do they impact galactic cosmic rays and solar energetic particle fluxes?

SQ 2.2 What is the impact of the HCS properties and processes (e.g., magnetic reconnection and instabilities) on suprathermal particle energization and transport?

Addressing these questions requires determining the large and intermediate-scale structure of the HCS. To measure the possible eigenmodes of HCS oscillations and their impact on energetic particle transport requires multiple azimuthally and radially separated spacecraft with instrumentation to measure magnetic fields, thermal and suprathermal plasma, and their pitch-angle distributions.

MHD simulations from $r = 30R_\odot$ to 5 AU (Riley et al., 2002) and Wind observations at 1 AU (Linker et al., 1999) suggest that the latitude of the HCS is highly variable, typically ranging from −10 to 10° as a function of longitude. At the Venus orbit, at 0.7 AU, we expect to encounter the HCS from $Z_{GSE} \approx \pm 18$ Gm. The multi-scale, volumetric measurements during the first mission phase will allow the determination of the 3-D intermediate-scale structure and physical processes within the HCS. The large-scale azimuthal coverage during the last mission phase allows for the determination of the large-scale structure and motion of the HCS and the existence of possible eigenmodes. Surface eigenmodes have been detected on the Earth's magnetopause current layer (Archer et al., 2013). The experience and techniques from multi-point measurements through ISEE 1 and 2, Cluster, THEMIS, and MMS in the Earth's MSP can be used to guide and answer these science questions.

2.1.3 Stream interaction and co-rotating interaction regions

SIRs form when the high-speed SW from coronal holes overtakes the low-speed SW that has been emitted earlier such that the interaction between these two streaming plasmas creates a compressional interface that co-rotates with the Sun (Gosling et al., 1978). CIRs have been associated with the acceleration of protons above 1 MeV energy irrespective of whether bounding shocks were present or not, possibly by being scattered back and forth (Fermi acceleration) across the trailing edges of the compression regions by large-amplitude Alfvén waves (Desai et al., 1998). **Figure 3** shows an example of 8 h of observations of the CIR velocity shear interface revealing 100–140 km/s of velocity fluctuations as measured by Wind, ACE, and DSCOVR (DSC) at L1 separated by 60–80 R_E from each other along y_{GSE}. These fluctuations could be produced by various processes, e.g., 1) large-amplitude waves produced by shock processes or produced remotely but are just being convected to CIRs, 2) Kelvin–Helmholtz waves, or 3) mirror-mode waves. Since the Alfvén speed is only around a 10th of the SW speed at 1 AU, solar wind fluctuations are convected with the SW. Early observations have confirmed that these types of fluctuations are a common feature of co-rotating high-speed streams (Smith et al., 1995), and they can increase in amplitude when convected in the interaction region (Tsurutani et al., 1995). When these measurements from three spacecraft are injected into a recently developed multi-spacecraft

SW monitor interpolation technique (Burkholder et al., 2020a), the scale sizes of the magnetic field (e.g., B_z) and plasma (e.g., V_z and n) can be estimated. **Figure 3** reveals a highly structured SW at the 20–80 R_E scale along the X_{GSE} and Y_{GSE} direction, which is comparable to the scale, the size of the dayside MSH–MSP system along the Y_{GSM} direction.

This structure would affect the shock geometry on Earth and the properties of the magnetopause impacting the onset conditions and driving various processes at the MSH and magnetopause (Nykyri, 2013; Hietala et al., 2018; Burkholder et al., 2020b; Nykyri, 2020; Nykyri et al., 2021a; Nykyri et al., 2021b).

The major science questions are as follows:

SQ 3.1 What processes are responsible for plasma and magnetic field fluctuations at SIRs/CIRs?

SQ 3.2 How does the CIR/SIR structure evolve from 0.7 AU to 1 AU, and how do CIR properties impact SW–MSP coupling processes?
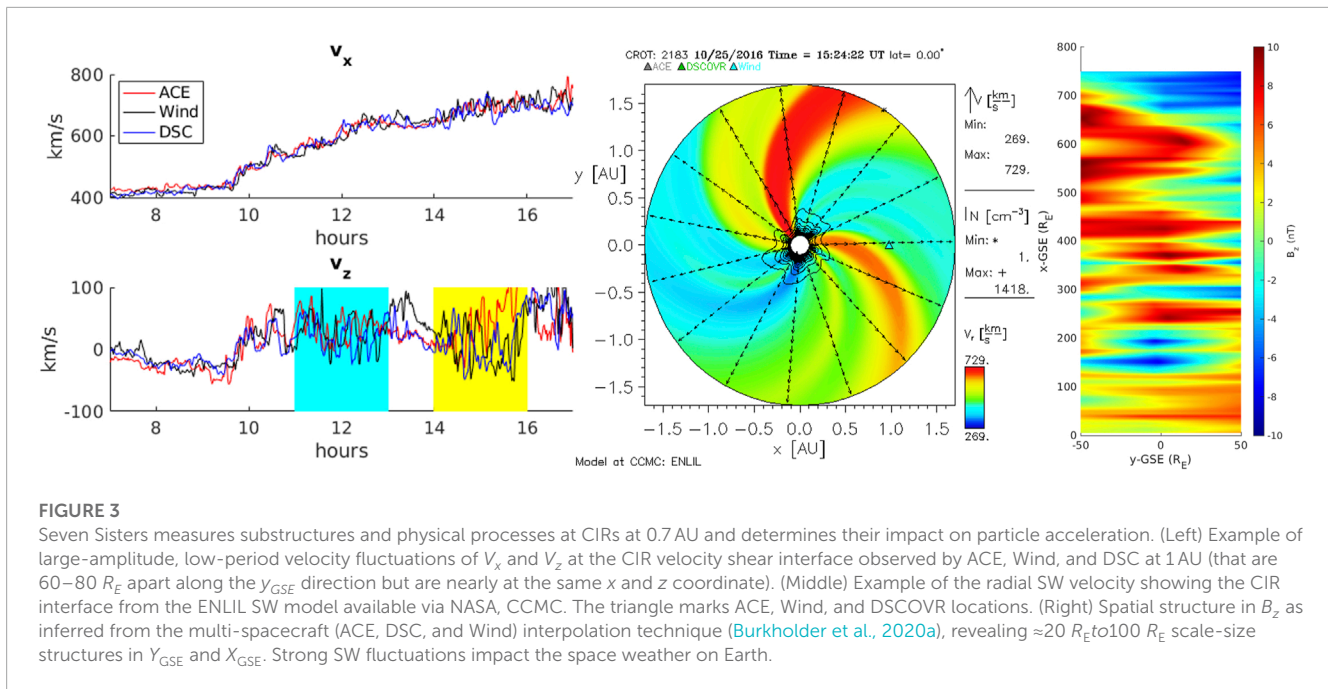
SQ 3.3 What are the detailed particle acceleration mechanisms at SIRs/CIRs?

In order to predict, 1–2 days in advance, the conditions that are likely to generate this type of structured SW at scale sizes comparable to the Earth's magnetospheric system, we need measurements at $r < 1$ AU. The Seven Sisters at 0.7 AU would provide > 50 days/Earth-year of 31 h advanced measurements of CIR structures likely to hit the Earth. Furthermore, a comparison of Seven Sisters data at the geo-effective region (GER, see **Figure 5**) with EL1 missions would allow the determination of the evolution of CIRs.

2.1.4 Solar wind flux tubes and periodic density structures

SWFTs have often been identified at 1 AU by spotting the flux tube walls with large changes in the magnetic field direction and the flow velocity (Borovsky, 2008). The tube walls were associated with large changes in the ion-specific entropy and the alpha-to-proton ratio. The median flux tube diameter (d_{FT}) is about 560 Mm and was observed to be larger in the slow SW than in the fast SW. The tubes are on-average aligned with the Parker spiral, with a large spread in orientations. Understanding the properties and evolution of SWFTs is important, as they can guide the motion of the energetic particles, and the associated SWFT plasma and magnetic field properties affect the efficiency of the solar wind–magnetosphere–ionosphere coupling processes. As the SW is expanding, it may be difficult for flux tubes to reconnect with each other and dissipate due to the thickness of flux tube boundaries (Borovsky, 2008).

Because the SW is a magnetized fluid, it is surprising that the inertial range spectral index at $r = 1$ AU satisfies the hydrodynamic Kolmogorov scaling with a slope of −5/3 (Kolmogoroff, 1941). In MHD, oppositely propagating fluctuations can give rise to a turbulent energy cascade due to non-linear interactions. If a strong magnetic field is applied, the cascade is suppressed in the direction of the magnetic field and one could get the −3/2 power law (Kraichnan, 1965). Multi-SC measurements within individual SWFTs at scales below d_{FT} are required to separate the effects of SWFT boundaries on magnetic power spectra and determine whether the turbulence within individual flux tubes at $r = 1.0$ AU satisfies the −3/2 power law. Interestingly, the inertial range spectral index for the magnetic field at distances from the Sun lower than 0.6 AU is approximately −3/2 (Chen et al., 2020). Due to a more radial alignment of SWFTs

FIGURE 3
Seven Sisters measures substructures and physical processes at CIRs at 0.7 AU and determines their impact on particle acceleration. (Left) Example of large-amplitude, low-period velocity fluctuations of V_x and V_z at the CIR velocity shear interface observed by ACE, Wind, and DSC at 1 AU (that are $60-80\ R_E$ apart along the y_{GSE} direction but are nearly at the same x and z coordinate). (Middle) Example of the radial SW velocity showing the CIR interface from the ENLIL SW model available via NASA, CCMC. The triangle marks ACE, Wind, and DSCOVR locations. (Right) Spatial structure in B_z as inferred from the multi-spacecraft (ACE, DSC, and Wind) interpolation technique (Burkholder et al., 2020a), revealing $\approx 20\ R_E\ to\ 100\ R_E$ scale-size structures in Y_{GSE} and X_{GSE}. Strong SW fluctuations impact the space weather on Earth.

closer to the Sun, this may be indicative of the possible localization of measurements within individual SWFTs. To assess the general properties of turbulence and its evolution, it would be important to have multi-point measurements at 0.6 AU $<r<1$ AU to measure the spectral indices and their evolution within individual SWFTs. While it may not be the primary science objective, Seven Sisters two-scale tetrahedron measurements in the geo-effective region would also provide important information of the SW turbulence, which can then be compared to those closer to the Earth, e.g., with a HelioSwarm-type of mission.

PDSs are sometimes associated with SWFTs (Di Matteo et al., 2019; Kepko et al., 2020). PDSs manifest as quasi-periodic fluctuations of the SW density ranging from a few minutes to a few hours. Based on the average SW velocity, PDSs have radial length scales greater than or equal to the size of the Earth's dayside MSP (≈ 100 Mm–10 Gm). PDSs have been mostly observed in the solar atmosphere in remote imaging data (Viall et al., 2010; Viall and Vourlidas, 2015; DeForest et al., 2018) and *in situ* measurements at 1 AU (Viall et al., 2009; Kepko et al., 2020). Only few instances of PDSs have been reported at 0.3, 0.4, and 0.6 AU based on single spacecraft observations (Di Matteo et al., 2019). Evidence of elemental and ionic compositions and charge-state ratios at similar periodicities connect PDSs to processes in the solar corona (Kepko et al., 2016; Gershkovich et al., 2022). PDSs observed at the HCS can be associated with SWFTs ejected from the tip of helmet streamers (Viall et al., 2010), consistent with recent simulations and laboratory experiments showing that the tearing instability and magnetic reconnection at the tip of the helmet streamer can release coronal plasma in a quasi-periodic manner (Réville et al., 2020; Peterson et al., 2021). However, the percentage of PDSs of a solar origin as opposed to the ones formed by *in situ* processes is an open question. Additionally, as most observations of PDSs came from single spacecraft measurements, their 3-D properties are not understood.

The science questions of interest are as follows:

SQ 4.1 What are the SWFT properties at 0.7 AU and how does the SWFT modify energetic particle propagation?
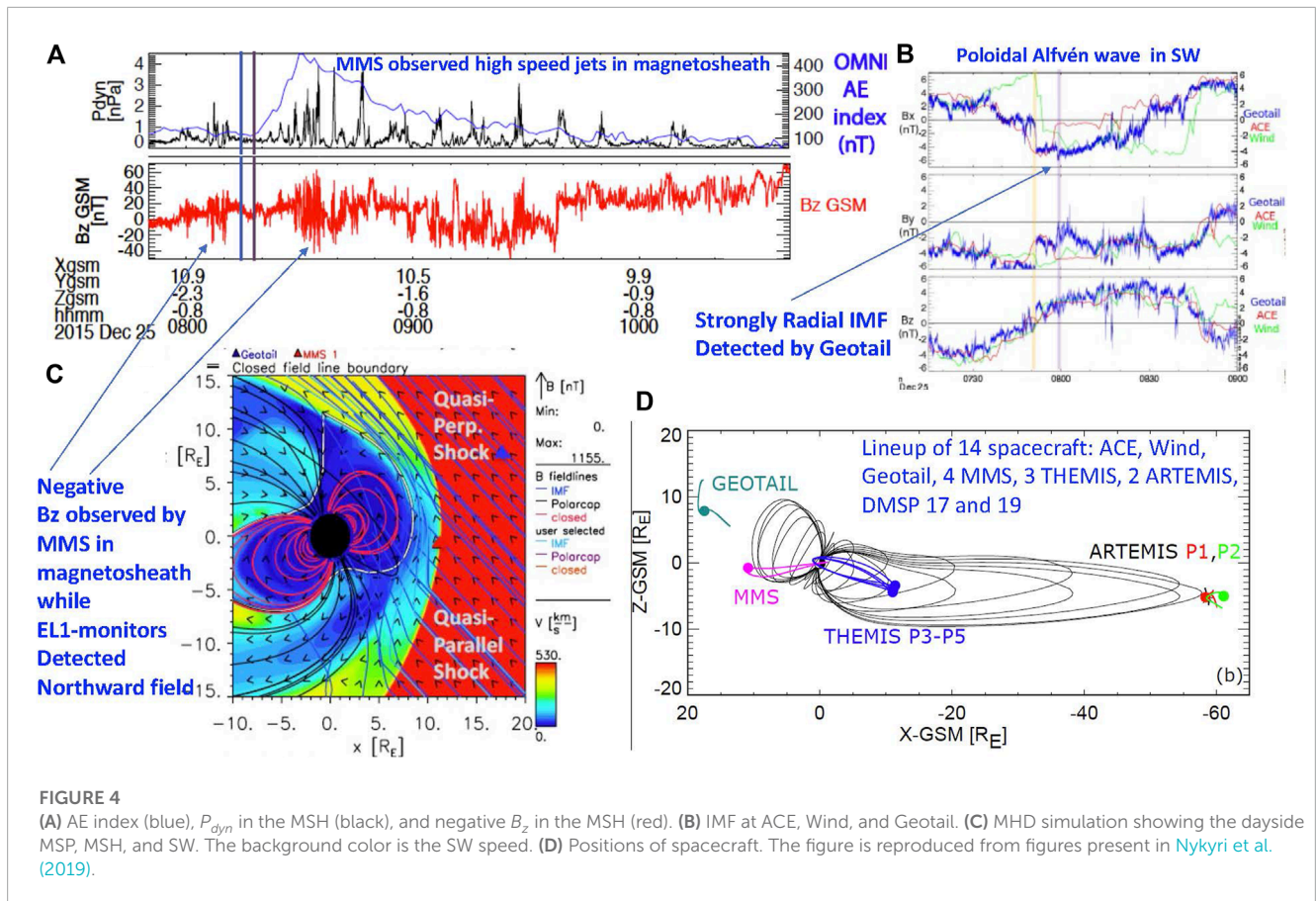
SQ 4.2 How well is the ion-specific entropy conserved within individual SWFTs, and what are the non-adiabatic processes within SWFTs changing the specific entropy?

SQ 4.3 How are PDSs formed, what are their properties, and how do they evolve?

SQ 4.4 Does the turbulent spectra at 0.7 AU within individual SWFTs follow the $-3/2$ or $-5/3$ power law? How does the turbulence evolve from 0.7 AU to 1 AU?

SQ 4.5 Is the turbulence predominantly Alfvénic or highly anisotropic and dominated by 2-D fluctuations?

These questions can be resolved by volume measurements by >4 SC constellations at appropriate scales. The suprathermal composition measurements of [[eqnstart1]], [[eqnstart2]], and [[eqnstart3]] as well as calculations of the specific entropy of the thermal plasma will allow identification of flux tube walls, as these quantities change rapidly when crossing from one SWFT to another (Borovsky, 2008). Pitch-angle measurements of the energetic particles are also needed, and these are expected to change when crossing flux tube boundaries revealing their effect on energetic particle scattering. During SWFT boundary crossings, it is also important to determine the nature of the discontinuity, e.g., rotational or tangential and the related properties that also regulate dayside transient phenomena in the Earth's MSP (Zhang et al., 2022). Simultaneous two-point composition measurements of SWFT/PDS properties at three different azimuthal separations (at VL-1, VL-4, and VL-5) would also reveal the variability of the processes at the solar surface and coronal processes of the solar plasma release as charge-state ratios do not change after reaching the collision-less regime at the freeze-in point (Gershkovich et al., 2022). Multi-SC studies will also unveil information about the actual size scales of PDSs, currently still an open question. Engulfing the

FIGURE 4
(A) AE index (blue), P_{dyn} in the MSH (black), and negative B_z in the MSH (red). **(B)** IMF at ACE, Wind, and Geotail. **(C)** MHD simulation showing the dayside MSP, MSH, and SW. The background color is the SW speed. **(D)** Positions of spacecraft. The figure is reproduced from figures present in Nykyri et al. (2019).

dayside MSP, PDSs can lead to compressional fluctuations of the Earth's magnetic field at a similar frequency (≈0.2–4.0 mHz). The periodic nature of these structures, especially when observed within SIRs (Kepko and Viall, 2019), has important consequences for the Earth's MSP dynamics, particularly involving radiation belt electrons (Breneman et al., 2020; Di Matteo et al., 2022).

2.1.5 Magnetohydrodynamic (MHD) waves

While the SW flow typically (except at CIR structures) is supermagnetosonic, a spectrum of MHD waves (Alfvén, slow, and fast) can be convected by the SW flow, and they can affect the plasma and IMF properties on Earth. Based on the nearly incompressible MHD theory in the $\beta < 1$ or $\beta \sim 1$ regime, turbulence can be regarded as a superposition between 2-D and slab (Alfvénic) turbulence. The large-wavelength (40 Mm–2 Gm) poloidal and toroidal IMF fluctuations superposed on average the Parker-spiral IMF can affect energetic particle propagation in the SW and impact energetic particle properties in the Earth's MSH, directly through acceleration processes at the quasi-parallel shock.

Recently, it has been shown by 14-spacecraft observations (see Figure 4), how a large-scale (≈2 Gm in wavelength) poloidal IMF oscillation triggered magnetotail reconnection and a geomagnetic substorm with Pi2 pulsations and auroral activity at the high-latitude ionosphere (Nykyri et al., 2019). A southward IMF interval during this poloidal oscillation first allowed the accumulation of magnetic flux into the magnetotail. The subsequent radial IMF interval, detected by Geotail but missed by Earth–Sun Lagrange 1 (EL1 monitors) produced high-speed jets (HSJs), which generated

−30 nT negative B_z in the MSH, despite the fact that SW monitors at EL1 measured a northward IMF (see Figure 4 and the caption). The southward field carried by HSJs triggered transient dayside reconnection, which was confirmed by DMSP data. The AE index (Figure 4A) increased after the first group of HSJs and likely resulted in critical flux enhancement into the magnetotail, which ultimately resulted in tail reconnection and substorm onset (Nykyri et al., 2019).

Fast mode waves can be created by various SW perturbations. Depending on the scale size and nature of the perturbation and distance from the Earth, they can affect plasma properties on Earth (Nykyri et al., 2017; Piersanti et al., 2022; Villante et al., 2022). Our recent simulation results (manuscript in preparation) have shown that when the "cone of influence" of the perturbation does not encompass the location of the observing spacecraft, the geo-effective space weather driver may be fully missed, even if the spacecraft is directly upstream of the Sun–Earth line.

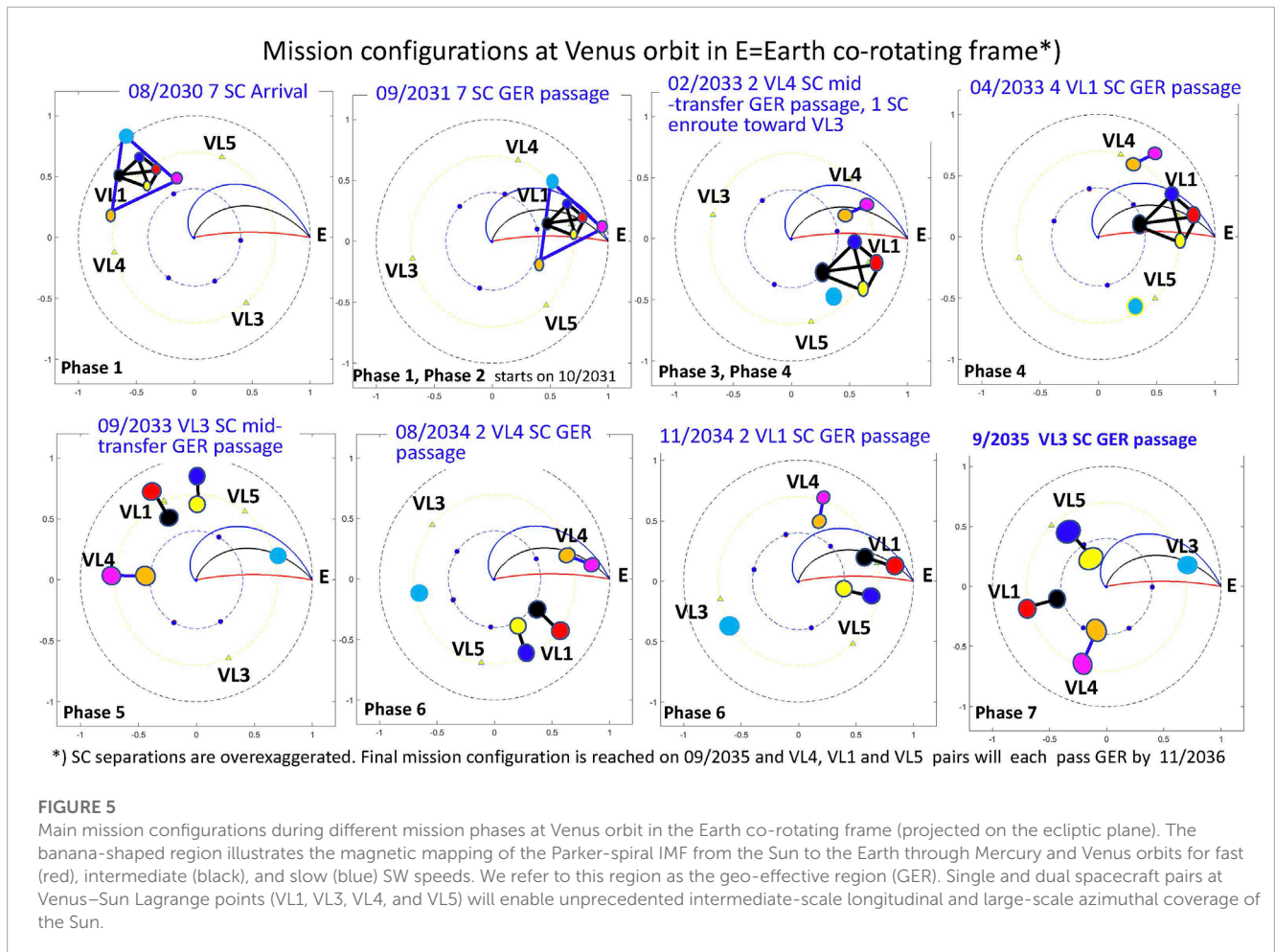The major science questions are as follows:

SQ 5.1 Knowing the spectra and properties of the large-scale solar wind fluctuations at 0.7 AU in the GER, to what accuracy can IMF orientation at EL1 and at Earth's bow shock be predicted 1–2 days in advance?

SQ 5.2 What are the wavelengths that can survive the 0.3 AU travel from the GER at Venus orbit to the Earth's?

SQ 5.3 Is the motion of SWFTs Alfvénic or are Alfvén waves localized and conducted by the SWFT?

SQ 5.4 Knowing the plasma conditions, magnetic field, and the spectra and properties of fast mode waves at 0.7 AU in the GER, to

FIGURE 5
Main mission configurations during different mission phases at Venus orbit in the Earth co-rotating frame (projected on the ecliptic plane). The banana-shaped region illustrates the magnetic mapping of the Parker-spiral IMF from the Sun to the Earth through Mercury and Venus orbits for fast (red), intermediate (black), and slow (blue) SW speeds. We refer to this region as the geo-effective region (GER). Single and dual spacecraft pairs at Venus–Sun Lagrange points (VL1, VL3, VL4, and VL5) will enable unprecedented intermediate-scale longitudinal and large-scale azimuthal coverage of the Sun.

what accuracy can the magnetic field strength and plasma density at EL1 and at Earth's bow shock be predicted 1–2 days in advance?

To determine the plasma frame frequency, wave number (**k**-vector), phase, and amplitude of the MHD wave spectrum requires at least two SC closely aligned along **k**, a vector with SC separations less than the wave coherence scale (Moore et al., 2016; Nykyri et al., 2021b). To improve our prediction of the IMF orientation, especially B_z, on Earth, it is important to determine the spectra of MHD waves at 0.7 AU at different Z_{GSE} and Y_{GSE} coordinates and to validate with EL1 spacecraft how accurately this can be carried out, and what are the minimum wavelengths that survive the convection of the 0.3 AU distance from Venus's orbit to the Earth's. With seven SC, one can create 21 two-SC combinations, maximizing the probability of the **k** vector alignment between the two SC. The early mission phase of the Seven Sisters with two nested tetrahedrons is ideal for tackling this problem and opening new possibilities for the development and use of new multi-spacecraft analysis techniques (Vogt et al., 2008; Zhang et al., 2022).

3 Seven Sisters mission overview

Motivated by these science questions and especially by the need to better understand the physical mechanisms within and the

radial development of various SW structures (e.g., the 3-D and longitudinal structure and evolution of CMEs, MHD wave spectra, and SIRs), we propose a first of its kind Pathfinder mission (Seven Sisters).

The mission will first fly as a seven SC, tetrahedron constellation at two different scales along the Venus–Sun Lagrange 1 point (VL1). This seven SC tetrahedron will travel through the geo-effective region in September 2031, after which three SC will start their journey toward VL4 and VL5. The four spacecraft tetrahedron will go through the GER in April 2033. These multi-SC GER passages are ideal for developing and testing space weather forecasting tools.

At a later mission phase, SC will occupy Venus–Sun Lagrange points (two at VL1, VL4, and VL5 and one at VL3) to enable the study of the azimuthal and longitudinal variation of CMEs, SIRs, HCSs, SWFTs/PDSs, properties of large-scale ($\lambda > 40$ Mm–2 Gm) MHD waves, and particle transport and acceleration.

This mission will provide > 50 days/Earth year (≈550 days during the 7-year mission) of up to 1–2-day advanced warnings of space weather phenomena when one or more of the Venus–Sun Lagrange points lie sunward from the Earth and/or further toward the western limb of the Sun at the GER. This will enable the development of improved models resulting in advanced predictions of geo-effective phenomena and IMF orientations on Earth.

3.1 Seven Sisters science goals and objectives

The Seven Sisters primary science goals (SG) and objectives (SO) are toSG 1: Determine the structure and evolution of the solar wind needed to develop a prototype next-generation monitoring system capable of predicting extreme and dynamic conditions in space up to 2 days before they reach the Earth.**SO 1.1:** Determine the 3-D, large-scale (0.6 AU–1.2 AU) to intermediate-scale (≈ 2 Mmto100 Mm) azimuthal and longitudinal structure of CMEs.

SO 1.2: Determine the 3-D, large- to intermediate-scale structure of HCSs, SIRs, and SWFTs/PDSs.

SO 1.3: Ascertain the evolution of CMEs, large-scale Alfvén waves, SWFTs/PDSs, and the associated radiation environment, from 0.7 AU to 1 AU.

SG 2: Reveal the role of the fundamental, multi-scale, physical processes associated with particle energization and transport in the solar wind structures.

SO 2.1: Identity the physical processes critical for particle acceleration and transport in CMEs, HCSs, SIRs, and SWFTs.

SO 2.2: Quantify the relative importance of the different physical mechanisms for particle acceleration and transport in CMEs, HCSs, SIRs, and SWFTs.

3.2 Schedule and science phases

The Seven Sisters mission will have seven main mission phases. These phases and target science objectives are listed in the following paragraphs, with spacecraft configurations depicted (not to scale) in **Figure 5**. Currently, mission engineering has been designed for the November 2029 launch, but this can be adjusted. During the mission, SC will travel through the GER at $Z_{GSE} = \pm 6$ Gm about the Earth–Sun ecliptic plane providing great coverage about the HCS, which can typically wobble between $Z_{GSE} = \pm 15$ Gm. This also allows us to compare properties and evolution of large-wavelength (≈ 2 Gm) Alfvénic fluctuations, CMEs, and SIRs at different Z_{GSE} at $X_{GSE} = 0.7$ AU–1 AU.

Launch: A total of seven identical SC carrying identical instrumentation (magnetometer, electrostatic analyzer, and energetic particle ([[eqnstart4]], [[eqnstart5]], and [[eqnstart6]]) detector) are launched simultaneously using the Falcon Heavy launch vehicle in November 2029. From the Earth's parking orbit, each spacecraft travels individually in a near string of pearls configuration and arrives at the Venus–Sun L1 (VL1) point in August, 2030. The spacecraft are separated ≈ 10 Mm–15 Mm from each other at this stage, enabling cruise phase science measurements of the SW before their arrival to VL1.

Phase 1: 8/2030–10/2031, seven SC nested constellations. They first fly as seven SC tetrahedron constellations about VL1 from August 2030 until October 2031. The four inner SC form closely an ideal tetrahedron with separations ranging from ≈ 1 Mm–15 Mm and the three outer spacecraft form a triangle with separations ranging from 15 Mm–80 Mm. This configuration allows the measurement of the structure and processes at the HCS and SIRs as well as probes the CME intermediate-scale structure. They make passage of the GER upstream the Earth (see second panel in **Figure 2**) from mid-8/2031 to early 10/2031 at

$Z_{GSE} = -6$ Gm. The SC separation of the four inner spacecraft during the GER passage is 15 Mm and the outer three is 80 Mm. The seven spacecraft volumetric measurements will also enable 21 two-SC combinations, maximizing the chances to determine the phase, amplitude, frequency, and k vector of MHD wave modes and allow the testing of how accurately the IMF B_z can be determined on Earth due to the superposition of poloidal Alfvén waves along the average Parker-spiral IMF. Target SOs: 1.2, 1.3, 2.1, and 2.2.

Phase 2: 10/13/2031–12/6/2031, six SC constellations, one VL3 SC departure from VL1. On 10/13/2031, VL3 SC starts its journey from VL1 toward VL3, requiring Venus gravity assists on 11/26/2031. To reduce the necessary propellant, the spacecraft does not enter into the orbit around VL3, instead performing a burn on 11/18/2034 to slow its velocity relative to VL3. It travels through the GER from 8/2033 to 10/3033 at $Z_{GSE} = 6.5$ Gm and 8/2035 to 10/2035 at $Z_{GSE} = 6$ Gm. Information theory (mutual information and transfer entropy) can be applied to these single spacecraft measurements at the GER together with Earth–Sun L1 measurements to study the propagation and dissipation of different scale SW structures. Meanwhile, the six SC constellations will continue volumetric measurements at VL1, and together with the "enroute VL3 SC" it will enable the measurement of large-scale structures. Target SOs: 1.1, 1.2, 1.3, 2.1, and 2.2.

Phase 3: 12/6/2031–8/28/2033, two VL4 SC departure from VL1. On 12/6/2031, two VL4 SC start their journey from VL1 toward VL4. They carry out a mid-transfer in the GER passage from 2/2033 to 3/3033 at $Z_{GSE} = 6$ Gm. They arrive at VL4 on 8/28/2033 and carry out the first VL4 in the GER passage on 7/2034 to 9/2034 at $Z_{GSE} = -6.75$ Gm and the second on 3/2036 to 4/2036 at $Z_{GSE} = 6$ Gm. Once at VL4, the SC separation is varied from 15 Mm–100 Mm enabling measurements of MHD wave mode properties during the GER. This configuration allows both intermediate- and large-scale measurements at the late mission phase when VL3, VL5, and VL1 will also be populated. Target SOs: 1.1, 1.2, and 1.3.

Phase 4: 12/6/2031–5/29/2033, four SC tetrahedrons at VL1. Four VL1 SC continue volumetric measurements at 15 Mm separations allowing the measurement of intermediate-scale properties of CMEs, HCSs, SIRs, SWFTs/PDSs, and MHD wave modes and together with three spacecraft in transit, they allow the measurement of large-scale structures. These four SC pass through the GER from 4/2033 through 5/2033 at $Z_{GSE} = 6$ Gm. Target SOs: 1.1, 1.2, 1.3, 2.1, and 2.2.

Phase 5: 5/29/2033–06/15/2035, two VL5 SC departure from VL1. On 5/29/2033, two VL5 SC start their journey from VL1 toward VL5, performing a Venus gravity assist on 10/10/2033. They carry out a mid-transfer in the GER passage from 1/2035 to 3/3035 at $Z_{GSE} = 6$ Gm. They arrive at VL5 on 6/15/2035 and carry out the VL5 GER passage on 9/2036 to 10/2036 at $Z_{GSE} = -6$ Gm. Once at VL5, the inter-SC separation is varied from 15 Mm–100 Mm enabling the measurements of MHD wave mode properties during the GER. This configuration allows both intermediate- and large-scale measurements at the late mission phase when VL3, VL4, and VL1 are also populated. Target SOs: 1.1, 1.2, and 1.3.

Phase 6: 8/28/2033–06/15/2035, two SC at VL1 and VL4, one enroute to VL3 and two enroute to VL5. The pairs at VL1 and VL4 enable intermediate-scale measurements from 15 Mm–50 Mm and together provide a large-scale measurement. VL1 SC carry out a

GER passage in late 10/2034 to mid-12/2034 (at ≈ 50 Mm scale) at $Z_{GSE} = -6$ Gm following the VL4 SC GER passage mentioned previously from late 7/2034 to mid-9/2034 (at ≈ 50 Mm scale). Target SOs: 1.1, 1.2, and 1.3.

Phase 7: 06/15/2035–12/2036, two SC at VL1, VL4, and VL5 and one close to VL3. In this mission phase, there is great azimuthal coverage of the Sun allowing measurements of both the intermediate- and large-scale HCS structure and the capturing of more CMEs. Inter-SC separations will be varied from 15 Mm–100 Mm for VL5 along the radial direction, which will make it possible to measure the intermediate and longitudinal structure of CMEs at 1 or more 0.6 AU azimuthally separated locations. At this stage, VL1 and VL4 SC separations will be varied from 50 Mm–100 Mm. By 11/2036, all SC pairs at VL1, VL4, and VL5 have completed their final GER passage. Target SOs: 1.1, 1.2, and 1.3.

At the possible extended mission phase from 1/2037 to 6/2037, we do not need station keeping but allow the SC to freely drift. The VL4–VL5 orbits are pretty stable, so we expect SC remain near these L-points, while SC at VL1 could fall away from VL1 either toward or away from Venus (and *vice versa* away/toward the Sun). The satellite near VL3 is in an elliptical orbit about the Sun, which is stable. This phase would enable (depending on the satellite motion) a study of the longitudinal structure of CMEs at a different scale than before. The science enhancing the cross-disciplinary benefit of the Seven Sisters mission is that VL1 SC will also provide a direct, upstream SW monitor for future Venus planetary missions or may even get closer to Venus in the extended mission phase.

## 3.3 Seven Sisters payload description

Past missions have provided very limited azimuthal coverage and even sparser out of the ecliptic coverage of the SW. The Seven Sisters will provide broad azimuthal coverage of the inner heliosphere as well as ±6 Gm out of ecliptic coverage. To achieve closure on science objectives, each of the seven SC carries identical instrumentation: a flux gate magnetometer (FGM) and an electrostatic analyzer (ESA), for thermal bulk ions (≤ 20 keV), and an energetic particle detector (EPD) for electrons, H$^+$ and He^{++} ions (≥ 20 keV to 5 MeV). FGM (burst mode) must have a sampling frequency of ≈ 12.5 Hz and the survey mode resolution needs to be ≈ 0.67 s to measure the passage of the current sheets (CS) with the minimum thickness of ≈ 1 Mm. To test which portion of the thin SW CS can be identified with the proposed instrument resolution, we have performed a statistical study of the SW CS properties, as identified with MMS burst-mode magnetic field data (128 Hz) between 2017 and 2018 (see example in **Figure 6**.), using previously published burst-mode intervals (Burkholder and Otto, 2019). The thicknesses varied from ≈ 0.1–3 Mm, and the maximum, minimum, and average crossing times of the CS, in this study, were 32.97, 0.16, and 3.08 s, respectively. If we use a 12.5 Hz sampling rate (0.08 s) data, there are 183 out of 183 cases (100%) that can be identified. If we use 1 Hz (1 s) data, 134 cases (73.22%) can be identified. Thus, it can be concluded that the burst-mode data of 12.5 Hz can even detect sub-1 Mm CSs and the survey mode of 1 Hz is sufficient to identify most of the CSs. ESA needs to measure the OMNI directional ion velocity distribution with a sampling rate of 0.125 Hz from few eV to 10 keV to be able to have enough measurements within the MHD wave mode wavelength, HCS thickness, and CME sheath thickness. The magnetic and plasma structure at SIRs at 1 AU has a scale size of ~ 10 R_E to 24.5 R_E. Both the tetrahedron phase and the later phase two-SC separations of 20 Mm–80 Mm are ideal for studying the formation of this structure. To study particle energization from thermal to suprathermal energies, the EPD needs to measure the energetic electrons, the energetic [[eqnstart9]] and [[eqnstart10]] ions (the dominant species in the SW) from thermal energies to at least ≈ 2 MeV, as well as construct pitch-angle distributions (PADs) from thermal to suprathermal energies within different SW substructures with a 10 s–60 s cadence.

3.4 Ground-based observatories and data transfer

The satellites will communicate with Earth through the Deep Space Network (DSN) and via the Ka frequency band. Daily communications will be necessary for the early mission phase to ensure all systems are working. Later, data need to be downlinked when the storage capacity is exceeded. Typically, approximately 4.5–6 h a week will be sufficient to ensure all of the science data collected is transferred. These communications are performed from distances as close as 0.25 AU and as far as 1.75 AU. The instruments collect significantly more data while in burst mode. Burst mode is initiated at GERs and will also be automatically initiated when the SC electronics circuit board response satisfies the ground-simulated "finger print" for specific solar wind transients (i.e., CMEs, SIRs, and HCSs). They enter this mode while in the GER, when impacted by a CME and when passing through a CIR or HCS. To estimate the amount of burst-mode data for costing analysis, we divided different mission phases into different predicted solar cycle phases and determined from published literature how many single spacecraft encounters at 1 AU or closer to Sun there have been with HCSs, CMEs, and CIRs. We also required the need to have burst mode when SC are traveling through the GER.

A simulation of data collection and transfer showed that in order to ensure all data collected by science instruments reach Earth, the satellites will each need a 2-m antenna. The data stored on board throughout the span of the mission is shown in **Figure 7**. There are segments, while a given satellite is close to Earth, that it is able to downlink more data than are stored. However, significant reductions in the antenna size make it impossible for all of the data to be transferred. The reduced data rates at the points furthest from the Earth cause such a large accumulation of data in the satellites that even the increased rates while close to the Earth are not capable of transferring all of the data present. The satellite then gains distance from the Earth without delivering all of the data it has on board, leading to an ever increasing data glut that can never be completely transferred. Therefore, the mission fuel/mass budget and associated cost estimate assume a 2-m antenna in each SC, which will enable the transfer of all the collected data back to the Earth. We have estimated that the total amount of science data during the 7-year mission to be ≈ is 3.2 TB.
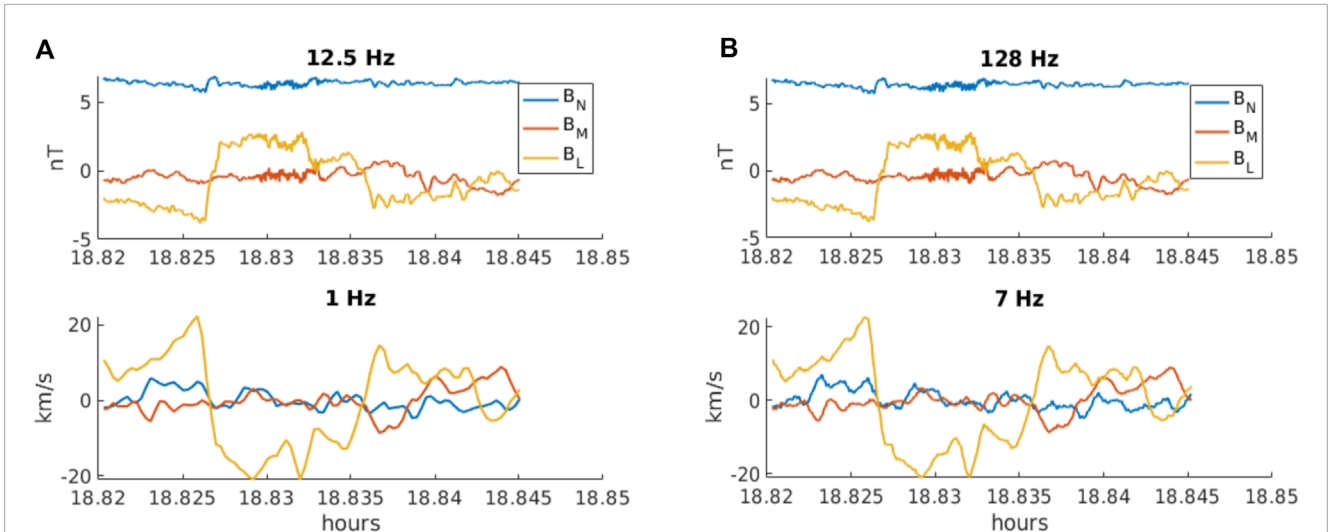
FIGURE 6
Example of an MMS observation of a 1.5-min interval of a reconnecting current sheet in the SW but downsampled to the proposed instrument magnetic field (12.5 Hz) and plasma (1 Hz) resolution. **(A)** Burst-mode (128 Hz and 7 Hz, respectively) identification of the same current sheet. **(B)** Results are in LMN coordinates and ion jets in the L direction are visible, corresponding to B_L reversal after the average SW speed has been extracted. Based on our MMS statistics of 183 current sheets, the proposed magnetic field instrumentation burst mode of 12.5 Hz can resolve all reconnecting SW thin current sheets identified with MMS burst-mode (128 Hz) data.
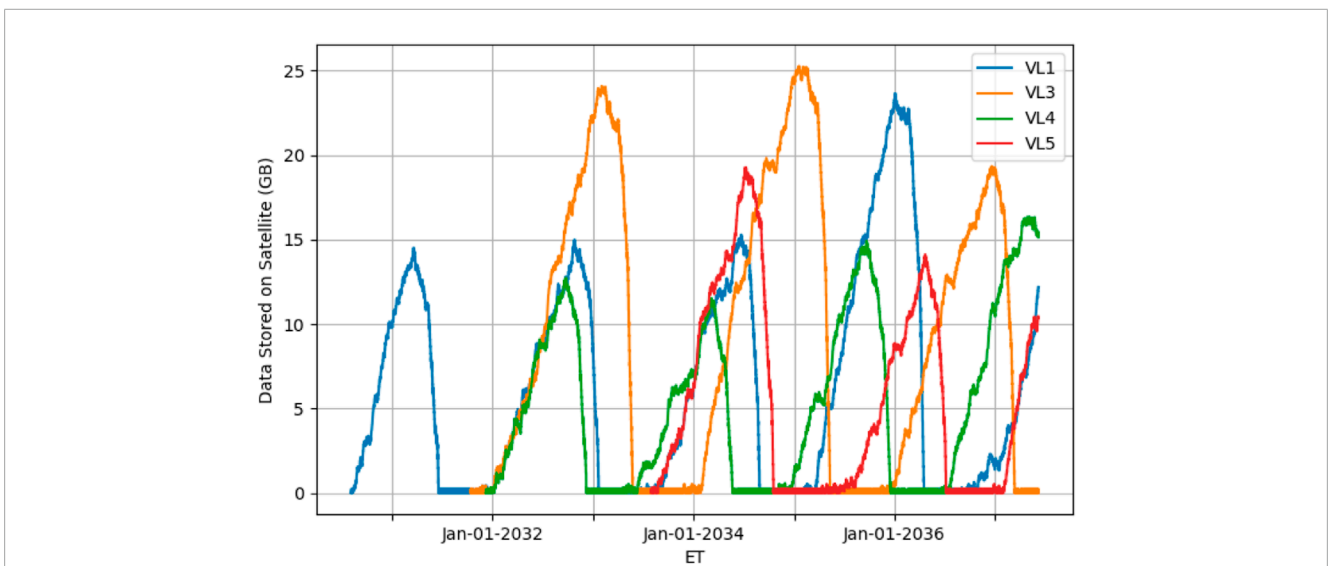
FIGURE 7
Simulated data stored in each satellite on the way to/at VL1, VL3, VL4, and VL5. Data accumulate while the satellite is particularly distant from the Earth and then declines sharply when that distance decreases and the possible data rate increases.

3.5 Key technologies and risks

Our mission science requirements can be fully accomplished with heritage instrumentation from Space Weather Follow On-Lagrange 1 (SWFO-L1) and IMAP, which will all be at TRL 9 at the time the Seven Sisters will be launched. There is considerable risk in using a single bus to transition from the Earth's parking orbit to Venus's parking orbit. Therefore, we fly the seven SC separately to VL1 point from the Earth's parking orbit, enabling cruise phase science and minimizing risks.

3.6 Descope options

A. If we need to reduce the cost, we could get rid of the VL3 satellite. This would reduce the simultaneous azimuthal coverage about the Sun, the time when we have a monitor upstream of the Earth, and the two-scale volumetric measurements in phase 1, however, a reasonable portion of the science would still be accomplished.

B. If the mission cannot launch and send the seven satellites at the same time, then the first four satellites can still provide a

≈ 10 Mm scale at the early stage, while waiting for the arrival of the remaining three satellites. However, a second launch would bring the cost up.

C. If the mission would be permanently cut to four satellites, then after a certain stage, the mission has to increase the separation of these four satellites to survey the larger scale structure. However, the mission would lose the chance to measure both intermediate- and large-scale structures simultaneously. Furthermore, in the later phase, each Lagrange point only has one satellite, which would not allow for the simultaneous comparison of particle distributions in different substructures, largely affecting the closure of our science objectives. In short, to successfully close all (most) the science objectives, we need a minimum of seven (six) spacecraft. Furthermore, in the rare event that there is no simultaneous Earth–Sun L1 monitor, the mission will need to launch an eighth identical spacecraft to the Earth–Sun L1 point or place the VL3 satellite into the Earth–Sun L1 orbit.

3.7 Cost estimate

Instrument costs, post launch science, and operations are based on heritage instrumentation from the SWFO-L1 for magnetometer (MAG) and ESA (SWiPS) and for IMAP for the energetic particle detector with composition measurements (CoDICE). The cost of SC busses is based upon the previous work completed by Advanced Space in SC assembly.

The estimated total cost for building the seven sets of TRL 9 level instruments of the MAG, ESA, and energetic particle detector with spares is $ 126 M. Presently, the cost for a single Falcon Heavy launch is $ 97 M. The SC busses are expected to cost between $ 35 M and $ 40 M each, based upon previous SC costing work completed by Advanced Space. The post launch science cost for instrumentation teams until January 2037 is $ 22.2 M, and post launch instrument operations, data-archiving, and ground system activities are estimated to be $ 24.5 M. The total expected mission cost, including the launch, is estimated to be $ 518.3 M–$ 557.8 M. A de-scoped six spacecraft mission would reduce the cost by $ 71.1 M to $ 79.9 M and provide additional savings in data transfer but a portion of the science objectives would not be met. To enable science engagement from a broad community, we also propose two NASA Heliophysics Guest Investigator (HGI) opportunities to optimize the science return during different mission phases, one for 2033 and one for 2037, which will be approximately $ 6 M each.

4 Conclusion and discussion

The heliosphere is our home in the Universe. Yet, considering its vast volume, our dynamic star and our technologically dependent society, far too little resources are currently devoted to acquiring multi-point, multi-scale, *in situ* measurements of it. For example, in atmospheric weather modeling, major advances in hurricane path forecasting have become available both due to increased radar and *in situ* probe measurements of wind speeds, densities, and pressures of a hurricane and its substructures. By the same analog, we need

more *in situ* and remote-sensing measurements of the solar wind and its transients.

Seven Sisters would be a multi-spacecraft mission, building on the successes and lessons learned from Cluster, MMS, and THEMIS. It will uncover and quantify the relative contribution of different physical mechanisms responsible for suprathermal particle acceleration in the solar wind structures. As it spends > 550 days in the GER upstream of the Earth, it will be an ideal mission to develop and test our tools for 1–2 days of advanced space weather forecasting.

However, this is just the first step. Adverse space weather conditions are not just a problem for the United States but for the entire world. During the next decades and beyond, we need to design a framework to mass-produce spacecraft instrumentation (both *in situ* and remote sensing) to allow multi-scale constellations at Mercury, Venus, and Earth Lagrange points, as well as at elliptical orbits about the Earth and the Sun. This can be achieved by collaborations between America, Europe, Africa, and Asia (including Australia).

Building and using a fully physics-based model from solar measurements for real-time space weather predictions is impossible. Like hurricane path forecasting, these multi-point measurements need to be fed in near real-time into global heliospheric models, which need to provide sufficiently well-resolved background fields, which can then be corrected by data from these multi-point measurements.

As a recommendation for funding agencies, we encourage the development of more funding and mentoring opportunities for mission concept development (both for science and engineering), so that smaller universities with little or no resources could also have a chance to develop critical infrastructure and workforce for space exploration. The Seven Sisters intends to be a ground-up developed, inclusive mission offering training and mentoring opportunities for early-career scientists from diverse backgrounds. If you want to get involved, contact any of the authors of this paper.

Data availability statement

THEMIS/ARTEMIS data is available at http://themis.ssl.berkeley.edu and all MMS data were downloaded through the MMS Science Data Center accessible at https://lasp.colorado.edu/mms/sdc/public/, and we recognize the efforts from MMS instrument teams and all who contribute to this service. SPEDAS software was used for THEMIS/MMS data processing and is available at http://spedas.org/wiki. All OMNI data can be accessed from NASA/GSFC's Space Physics Data Facility's OMNIWeb service at https://omniweb.gsfc.nasa.gov/. ACE, Wind, DSCOVR, MMS, and THEMIS data are available from Coordinated Data Analysis Web at https://cdaweb.gsfc.nasa.gov/index.html/. The MHD simulation result of CIR has been provided by the Community Coordinated Modeling Center at Goddard Space Flight Center through their public Runs on Request system (http://ccmc.gsfc.nasa.gov). The CCMC is a multi-agency partnership between NASA, AFMC, AFOSR, AFRL, AFWA, NOAA, NSF and ONR.

Author contributions

KN has been leading the Seven Sisters mission development and wrote the original manuscript, performed CME and Alfvén wave analyses in the SW, estimated DNS data transfer cost, and compiled **Figures 1–4**. BB performed CIR analysis and MMS current sheet analysis in **Figure 6**. Y-LL carried out the statistical study of current sheets with different sampling resolutions. RC provided initial SC stability analysis and orbit visualizations. JP, MR, and LM provided mission engineering analysis and provided **Figure 7** of the simulated data transfer. RE, MA, and KO provided instrument specifications for mission engineering and cost analysis. All co-authors have read and commented on the text. All authors contributed to the article and approved the submitted version.

Funding

Conflict of interest

JP, MR, and LM were employed by Advanced Space LLC.

The remaining authors declare that the research was conducted in the absence of any commercial or financial relationships that could be construed as a potential conflict of interest.

Publisher's note

All claims expressed in this article are solely those of the authors and do not necessarily represent those of their affiliated organizations, or those of the publisher, the editors, and the reviewers. Any product that may be evaluated in this article, or claim that may be made by its manufacturer, is not guaranteed or endorsed by the publisher.

References

Abbo, L., Ofman, L., Antiochos, S. K., Hansteen, V. H., Harra, L., Ko, Y. K., et al. (2016). Slow solar wind: Observations and modeling. *Space Sci. Rev.*201, 55–108. doi:10.1007/s11214-016-0264-1

Adhikari, L., Zank, G. P., Bruno, R., Telloni, D., Hunana, P., Dosch, A., et al. (2015). The transport of low-frequency turbulence in astrophysical flows. II. Solutions for the super-alfvénic solar wind. *Astrophysical J.*805, 63. doi:10.1088/0004-637X/805/1/63

Adhikari, L., Zank, G. P., and Zhao, L. L. (2020). A solar coronal hole and fast solar wind turbulence model and first orbit parker solar probe (PSP) observations. *ApJ*901, 102. doi:10.3847/1538-4357/abb132

Archer, M. O., Hartinger, M. D., and Horbury, T. S. (2013). Magnetospheric "magic" frequencies as magnetopause surface eigenmodes. *Geophys. Res. Lett.*40, 5003–5008. doi:10.1002/grl.50979

Bale, S. D., Kellogg, P. J., Mozer, F. S., Horbury, T. S., and Reme, H. (2005). Measurement of the electric fluctuation spectrum of magnetohydrodynamic turbulence. *Phys. Rev. Lett.*94, 215002. doi:10.1103/PhysRevLett.94.215002

Belcher, J. W., and Davis, L., Jr. (1971). Large-amplitude alfvén waves in the interplanetary medium, 2. *J. Geophys. Res.*76, 3534–3563. doi:10.1029/JA076i016p03534

Borovsky, J. E. (2008). Flux tube texture of the solar wind: Strands of the magnetic carpet at 1 AU?*J. Geophys. Res. (Space Phys.*113, 8110. doi:10.1029/2007JA012684

Breneman, A. W., Halford, A. J., Millan, R. M., Woodger, L. A., Zhang, X. J., Sandhu, J. K., et al. (2020). Driving of outer belt electron loss by solar wind dynamic pressure structures: Analysis of balloon and satellite data. *J. Geophys. Res. (Space Phys.*125, e28097. doi:10.1029/2020JA028097

Burkholder, B. L., Nykyri, K., Ma, X., Rice, R., Fuselier, S. A., Trattner, K. J., et al. (2020b). Magnetospheric multiscale observation of an electron diffusion region at high latitudes. *Geophys. Res. Lett.*47, e2020GL087268. doi:10.1029/2020gl087268

Burkholder, B. L., Nykyri, K., and Ma, X. (2020a). Use of the l1 constellation as a multispacecraft solar wind monitor. *J. Geophys. Res. Space Phys.*125, e2020JA027978. doi:10.1029/2020ja027978

Burkholder, B. L., and Otto, A. (2019). Magnetic reconnection of solar flux tubes and coronal reconnection signatures in the solar wind at 1 au. *J. Geophys. Res. Space Phys.*124, 8227–8254. doi:10.1029/2019JA027114

Chen, C. H. K., Bale, S. D., Bonnell, J. W., Borovikov, D., Bowen, T. A., Burgess, D., et al. (2020). The evolution and role of solar wind turbulence in the inner heliosphere. *Astrophysical J. Suppl. Ser.*246, 53. doi:10.3847/1538-4365/ab60a3

Crooker, N. U., Huang, C.-L., Lamassa, S. M., Larson, D. E., Kahler, S. W., and Spence, H. E. (2004). Heliospheric plasma sheets. *J. Geophys. Res. Space Phys.*109, A03107. doi:10.1029/2003JA010170

Crooker, N. U., Siscoe, G. L., Shodhan, S., Webb, D. F., Gosling, J. T., and Smith, E. J. (1993). Multiple heliospheric current sheets and coronal streamer belt dynamics. *J. Geophys. Res. Space Phys.*98, 9371–9381. doi:10.1029/93JA00636

DeForest, C. E., Howard, R. A., Velli, M., Viall, N., and Vourlidas, A. (2018). The highly structured outer solar corona. *Astrophysical J.*862, 18. doi:10.3847/1538-4357/aac8e3

Desai, M. I., Marsden, R. G., Sanderson, T. R., Balogh, A., Forsyth, R. J., and Gosling, J. T. (1998). Particle acceleration at corotating interaction regions in the three-dimensional heliosphere. *J. Geophys. Res. Space Phys.*103, 2003–2014. doi:10.1029/97JA02529

Di Matteo, S., Viall, N. M., Kepko, L., Wallace, S., Arge, C. N., and MacNeice, P. (2019). Helios observations of quasiperiodic density structures in the slow solar wind at 0.3, 0.4, and 0.6 AU. *J. Geophys. Res. (Space Phys.*124, 837–860. doi:10.1029/2018JA026182

Di Matteo, S., Villante, U., Viall, N., Kepko, L., and Wallace, S. (2022). On differentiating multiple types of ULF magnetospheric waves in response to solar wind periodic density structures. *J. Geophys. Res. (Space Phys.*127, e2021JA030144. doi:10.1029/2021JA030144

Dimmock, A. P., Balikhin, M. A., and Walker, S. A. (2013). Dispersion of low frequency plasma waves upstream of the quasi-perpendicular terrestrial bow shock. *Ann. Geophys.*31, 1387–1395. doi:10.5194/angeo-31-1387-2013

Eriksson, S., Lavraud, B., Wilder, F. D., Stawarz, J. E., Giles, B. L., Burch, J. L., et al. (2016). Magnetospheric Multiscale observations of magnetic reconnection associated with Kelvin-Helmholtz waves. *Geophys. Res. Lett.*43, 5606–5615. doi:10.1002/2016GL068783

Fermo, R. L., Opher, M., and Drake, J. F. (2014). Magnetic reconnection in the interior of interplanetary coronal mass ejections. *Phys. Rev. Lett.*113, 031101. doi:10.1103/PhysRevLett.113.031101

Foullon, C., Verwichte, E., Nakariakov, V. M., Nykyri, K., and Farrugia, C. J. (2011). Magnetic kelvin-helmholtz instability at the Sun. *Astrophys. J. Lett.*729, L8. doi:10.1088/2041-8205/729/1/L8

Foullon, C., Verwichte, E., Nykyri, K., Aschwanden, M. J., and Hannah, I. G. (2013). Kelvin-Helmholtz instability of the CME reconnection outflow layer in the low corona. *Astrophys. J.*767, 170. doi:10.1088/0004-637X/767/2/170

Gershkovich, I., Lepri, S. T., Viall, N. M., Di Matteo, S., and Kepko, L. (2022). Periodic solar wind structures observed in measurements of elemental and ionic composition *in situ* at L1. *Astrophys. J.*933, 198. doi:10.3847/1538-4357/ac73ee

Goldstein, M. L., Roberts, D. A., and Fitch, C. A. (1994). Properties of the fluctuating magnetic helicity in the inertial and dissipation ranges of solar wind turbulence. *J. Geophys. Res.*99, 11519–11538. doi:10.1029/94ja00789

Gosling, J. T., Asbridge, J. R., Bame, S. J., and Feldman, W. C. (1978). Solar wind stream interfaces. *Sol. wind stream interfaces*83, 1401–1412. doi:10.1029/JA083iA04p01401

Henry, Z. W., Nykyri, K., Moore, T. W., Dimmock, A. P., and Ma, X. (2017). On the dawn-dusk asymmetry of the kelvin-helmholtz instability between 2007 and 2013. *J. Geophys. Res. Space Phys.*122, 888–911. doi:10.1002/2017JA024548

Herring, M. (2019). *Astrodynamics of the next generation space weather prediction mission*. Master's thesis, Embry-Riddle Aeronautical University.

Hietala, H., Phan, T. D., Angelopoulos, V., Oieroset, M., Archer, M. O., Karlsson, T., et al. (2018). *In situ* observations of a magnetosheath high-speed jet triggering magnetopause reconnection. *Geophys. Res. Lett.*45, 1732–1740. doi:10.1002/2017GL076525

Jokipii, J. R., and Levy, E. H. (1977). Effects of particle drifts on the solar modulation of galactic cosmic rays. *Astrophys. J.*213, L85–L88. doi:10.1086/182415

Joyce, C. J., McComas, D. J., Schwadron, N. A., Vourlidas, A., Christian, E. R., McNutt, R. L., et al. (2021). Energetic particle evolution during coronal mass ejection passage from 0.3 to 1 au. *A&A*651. A2. doi:10.1051/0004-6361/202039933

Kahler, S. W., Sheeley, N. R., Jr., Howard, R. A., Koomen, M. J., Michels, D. J., McGuire, R. E., et al. (1984). Associations between coronal mass ejections and solar energetic proton events. *J. Geophys. Res. Space Phys.*89, 9683–9693. doi:10.1029/JA089iA11p09683

Kavosi, S., Spence, H. E., Fennell, J. F., Turner, D. L., Connor, H. K., and Raeder, J. (2018). Mms/feeps observations of electron microinjections due to kelvin-helmholtz waves and flux transfer events: A case study. *J. Geophys. Res. Space Phys.*123, 5364–5378. doi:10.1029/2018JA025244

Kay, C., dos Santos, L. F. G., and Opher, M. (2015). Constraining the masses and the non-radial drag coefficient of a solar coronal mass ejection. *Astrophysical J. Lett.*801, L21. doi:10.1088/2041-8205/801/2/L21

Kepko, L., Viall, N. M., Antiochos, S. K., Lepri, S. T., Kasper, J. C., and Weberg, M. (2016). Implications of l1 observations for slow solar wind formation by solar reconnection. *Geophys. Res. Lett.*43, 4089–4097. doi:10.1002/2016GL068607

Kepko, L., and Viall, N. M. (2019). The source, significance, and magnetospheric impact of periodic density structures within stream interaction regions. *J. Geophys. Res. (Space Phys.*124, 7722–7743. doi:10.1029/2019JA026962

Kepko, L., Viall, N. M., and Wolfinger, K. (2020). Inherent length scales of periodic mesoscale density structures in the solar wind over two solar cycles. *J. Geophys. Res. (Space Phys.*125, e28037. doi:10.1029/2020JA028037

Kilpua, E. K. J., Good, S. W., Dresing, N., Vainio, R., Davies, E. E., Forsyth, R. J., et al. (2021). Multi-spacecraft observations of the structure of the sheath of an interplanetary coronal mass ejection and related energetic ion enhancement. *Astron. Astrophys.*656, A8. doi:10.1051/0004-6361/202140838

Kilpua, E., Koskinen, H. E. J., and Pulkkinen, T. I. (2017). Coronal mass ejections and their sheath regions in interplanetary space. *Living Rev. Sol. Phys.*14, 5. doi:10.1007/s41116-017-0009-6

Kolmogoroff, A. N. (1941). The local structure of turbulence in incompressible viscous fluid for very large Reynolds number. *Dokl. Akad. Nauk. SSSR*30, 301–305.

Kraichnan, R. H. (1965). Inertial-range spectrum of hydromagnetic turbulence. *Phys. Fluids*8, 1385–1387. doi:10.1063/1.1761412

Leamon, R. J., Smith, C. W., Ness, N. F., Matthaeus, W. H., and Wong, H. K. (1998). Observational constraints on the dynamics of the interplanetary magnetic field dissipation range. *J. Geophys. Res.*103, 4775–4787. doi:10.1029/97ja03394

Linker, J. A., Mikić, Z., Biesecker, D. A., Forsyth, R. J., Gibson, S. E., Lazarus, A. J., et al. (1999). Magnetohydrodynamic modeling of the solar corona during whole Sun month. *Sun Mon.*104, 9809–9830. doi:10.1029/1998JA900159

Ma, X., Nykyri, K., Dimmock, A., and Chu, C. (2020). Statistical study of solar wind, magnetosheath, and magnetotail plasma and field properties: 12+ years of themis observations and mhd simulations. *J. Geophys. Res. Space Phys.*125, e2020JA028209. doi:10.1029/2020ja028209

Marsch, E., and Goldstein, H. (1983). The effects of coulomb collisions on solar wind ion velocity distributions. *J. Geophys. Res. Space Phys.*88, 9933–9940. doi:10.1029/JA088iA12p09933

Miura, A., and Pritchett, P. L. (1982). Nonlocal stability analysis of the MHD Kelvin-Helmholtz instability in a compressible plasma. *J. Geophys. Res.*87, 7431–7444. doi:10.1029/JA087iA09p07431

Moore, T., and Nykyri, K. (2017). Statistical Study of ion-scale wave properties during Kelvin-Helmholtz activity. *J. Geophys. Res.* submitted. doi:10.1016/j.asr.2015.09.013

Moore, T. W., Nykyri, K., and Dimmock, A. P. (2016). Cross-scale energy transport in space plasmas. *Nat. Phys.*12, 1164–1169. doi:10.1038/NPHYS3869

Moore, T. W., Nykyri, K., and Dimmock, A. P. (2017). Ion-scale wave properties and enhanced ion heating across the low-latitude boundary layer during kelvin-helmholtz instability. *J. Geophys. Res. Space Phys.*122, 11,128–11,153. doi:10.1002/2017JA024591

NASA (2006). *Solar Sentinels: Report of the science and Technology definition team. Technical memorandum (TM) NASA/TM-2006-214137, 2006-01518-0*. Greenbelt, Maryland 20771: Goddard Space Flight Center.

Nykyri, K., Bengtson, M., Angelopoulos, V., Nishimura, Y., and Wing, S. (2019). Can enhanced flux loading by high-speed jets lead to a substorm? Multipoint detection of the christmas day substorm onset at 08:17 ut, 2015. *J. Geophys. Res. Space Phys.*124, 4314–4340. doi:10.1029/2018JA026357

Nykyri, K., and Foullon, C. (2013). First magnetic seismology of the CME reconnection outflow layer in the low corona with 2.5-D MHD simulations of the Kelvin-Helmholtz instability. *Geophys. Res. Lett.*40, 4154–4159. doi:10.1002/grl.50807

Nykyri, K. (2013). Impact of MHD shock physics on magnetosheath asymmetry and Kelvin-Helmholtz instability. *J. Geophys. Res. (Space Phys.*118, 5068–5081. doi:10.1002/jgra.50499

Nykyri, K., Johnson, J., Kronberg, E., Turner, D., Wing, S., Cohen, I., et al. (2021a). Magnetospheric multiscale observations of the source region of energetic electron microinjections along the duskside, high-latitude magnetopause boundary layer. *Geophys. Res. Lett.*48, e2021GL092466. doi:10.1029/2021gl092466

Nykyri, K., Laxman, A., Argall, M., Borovsky, J., Broll, J., Burkholder, B., et al. (2022b). *Critical solar wind measurements required for the next generation space weather prediction mission: Science motivation for the seven Sisters mission*. Washington, D:C: National Academies. White paper for decadal survey for solar and space physics (heliophysics) 2024-2033 http://surveygizmoresponseuploads.s3.amazonaws.com/fileuploads/623127/6920789/107-5548346d581dadb6652266d428a79739_WhitePaperScience_v2-2.pdf.

Nykyri, K., Ma, X., Burkholder, B., Rice, R., Johnson, J., Kim, E.-K., et al. (2021b). MMS observations of the multi-scale wave structures and parallel electron heating in the vicinity of the southern exterior cusp. *J. Geophys. Res. Space Phys.*126, e2019JA027698. doi:10.1029/2019JA027698

Nykyri, K., Ma, X., Dimmock, A., Foullon, C., Otto, A., and Osmane, A. (2017). Influence of velocity fluctuations on the kelvin-helmholtz instability and its associated mass transport. *J. Geophys. Res. Space Phys.*122, 9489–9512. doi:10.1002/2017ja024374

Nykyri, K., Otto, A., Lavraud, B., Mouikis, C., Kistler, L., Balogh, A., et al. (2006). Cluster observations of reconnection due to the Kelvin-Helmholtz instability at the dawn side magnetospheric flank. *Ann. Geophys.*24, 2619–2643. doi:10.5194/angeo-24-2619-2006

Nykyri, K., and Otto, A. (2001). Plasma transport at the magnetospheric boundary due to reconnection in Kelvin-Helmholtz vortices. *Geophys. Res. Lett.*28, 3565–3568. doi:10.1029/2001GL013239

Nykyri, K., Parker, J., De Moudt, L., Rosen, M., Cuellar, R., Herring, M., et al. (2022a). *Seven Sisters – a pathfinder mission to protect humanity from space weather*. Washington, D.C: National Academies. White paper for decadal survey for solar and space physics (heliophysics) 2024-2033 http://surveygizmoresponseuploads.s3.amazonaws.com/fileuploads/623127/6920789/206-5d12134c82d19aae688488d806a62088_Seven-Sisters-Space_Mission-Concept-Nykyri_NAS_Whitepaper.pdf.

Nykyri, K. (2020). *Structure and dynamics of the magnetosheath*. American Geophysical Union AGU, 117–133. chap. 7. doi:10.1002/9781119509592.ch7

Páez, A., Jatenco-Pereira, V., Falceta-Gonçalves, D., and Opher, M. (2017). Kelvin–helmholtz instability at the cme–sheath and sheath–solar-wind interfaces. *Astrophysical J.*851, 112. doi:10.3847/1538-4357/aa9753

Peterson, E. E., Endrizzi, D. A., Clark, M., Egedal, J., Flanagan, K., Loureiro, N. F., et al. (2021). Laminar and turbulent plasmoid ejection in a laboratory Parker Spiral current sheet. *J. Plasma Phys.*87, 905870410. doi:10.1017/S0022377821000775

Piersanti, M., Di Matteo, S., Zhima, Z., Yang, Y., Zhang, Z., Marcucci, M. F., et al. (2022). On the source of the anomalous ulf waves detected at both ground and space-borne data on 23 june 2020. *J. Geophys. Res. Space Phys.*127, e2021JA030044. doi:10.1029/2021ja030044

Rangel, R. C. (2020). *Optimization of spacecraft formations about Lagrange points for the next generation space weather prediction mission*. Master's thesis, Embry-Riddle Aeronautical University.

Réville, V., Velli, M., Rouillard, A. P., Lavraud, B., Tenerani, A., Shi, C., et al. (2020). Tearing instability and periodic density perturbations in the slow solar wind. *Astrophysical J.*895, L20. doi:10.3847/2041-8213/ab911d

Riley, P., Linker, J. A., and Mikić, Z. (2002). Modeling the heliospheric current sheet: Solar cycle variations. *J. Geophys. Res. (Space Phys.*107, 1136. doi:10.1029/2001JA000299

Sexton, E. S., Nykyri, K., and Ma, X. (2019). Kp forecasting with a recurrent neural network. *J. Space Weather Space Clim.*9, A19. doi:10.1051/swsc/2019020

Sheeley, J., N. R., Harvey, J. W., and Feldman, W. C. (1976). Coronal holes, solar wind streams, and recurrent geomagnetic disturbances: 1973 1976. *Sol. Phys.*49, 271–278. doi:10.1007/BF00162451

Smith, E. J., Balogh, A., Neugebauer, M., and McComas, D. (1995). Ulysses observations of Alfvén waves in the southern and northern solar hemispheres. *Geophys. Res. Lett.*22, 3381–3384. doi:10.1029/95GL03268

Smith, E. J. (2001). The heliospheric current sheet. *J. Geophys. Res. Space Phys.* 106, 15819–15831. doi:10.1029/2000JA000120

Sorathia, K. A., Merkin, V. G., Ukhorskiy, A. Y., Allen, R. C., Nykyri, K., and Wing, S. (2019). Solar wind ion entry into the magnetosphere during northward imf. *J. Geophys. Res. Space Phys.* 124, 5461–5481. doi:10.1029/2019JA026728

Sorathia, K. A., Merkin, V. G., Ukhorskiy, A. Y., Mauk, B. H., and Sibeck, D. G. (2017). Energetic particle loss through the magnetopause: A combined global MHD and test-particle study. *J. Geophys. Res. Space Phys.* 122, 9329–9343. doi:10.1002/2017JA024268

Tsurutani, B. T., Ho, C. M., Arballo, J. K., Goldstein, B. E., and Balogh, A. (1995). Large amplitude IMF fluctuations in corotating interaction regions: Ulysses at midlatitudes. *Ulysses A. T. midlatitudes* 22, 3397–3400. doi:10.1029/95GL03179

Viall, N. M., Kepko, L., and Spence, H. E. (2009). Relative occurrence rates and connection of discrete frequency oscillations in the solar wind density and dayside magnetosphere. *J. Geophys. Res. (Space Phys.* 114, A01201. doi:10.1029/2008ja013334

Viall, N. M., Spence, H. E., Vourlidas, A., and Howard, R. (2010). Examining periodic solar-wind density structures observed in the SECCHI heliospheric imagers. *Sol. Phys.* 267, 175–202. doi:10.1007/s11207-010-9633-1

Viall, N. M., and Vourlidas, A. (2015). Periodic density structures and the origin of the slow solar wind. *Astrophysical J.* 807, 176. doi:10.1088/0004-637x/807/2/176

Villante, U., Recchiuti, D., and Di Matteo, S. (2022). The transmission of ulf waves from the solar wind to the magnetosphere: An analysis of some critical aspects. *Front. Astronomy Space Sci.* 9. doi:10.3389/fspas.2022.835539

Vogt, J., Narita, Y., and Constantinescu, O. D. (2008). The wave surveyor technique for fast plasma wave detection in multi-spacecraft data. *Ann. Geophys.* 26, 1699–1710. doi:10.5194/angeo-26-1699-2008

Wilder, F. D., Ergun, R. E., Schwartz, S. J., Newman, D. L., Eriksson, S., Stawarz, J. E., et al. (2016). Observations of large-amplitude, parallel, electrostatic waves associated with the kelvin-helmholtz instability by the magnetospheric multiscale mission. *Geophys. Res. Lett.* 43, 8859–8866. doi:10.1002/2016GL070404

Wilder, F. D., Schwartz, S. J., Ergun, R. E., Eriksson, S., Ahmadi, N., Chasapis, A., et al. (2020). Parallel electrostatic waves associated with turbulent plasma mixing in the kelvin-helmholtz instability. *Geophys. Res. Lett.* 47, e2020GL087837. doi:10.1029/2020gl087837

Winterhalter, D., Smith, E. J., Burton, M. E., Murphy, N., and McComas, D. J. (1994). The heliospheric plasma sheet. *J. Geophys. Res. Space Phys.* 99, 6667–6680. doi:10.1029/93JA03481

Zank, G. P., Adhikari, L., Hunana, P., Shiota, D., Bruno, R., and Telloni, D. (2017). Theory and transport of nearly incompressible magnetohydrodynamic turbulence. *Theory Transp. Nearly Incompressible Magnetohydrodynamic Turbul.* 835, 147. doi:10.3847/1538-4357/835/2/147

Zank, G. P., Adhikari, L., Hunana, P., Tiwari, S. K., Moore, R., Shiota, D., et al. (2018). Theory and transport of nearly incompressible magnetohydrodynamic turbulence. IV. Solar coronal turbulence. *Sol. Coronal Turbul.* 854, 32. doi:10.3847/1538-4357/aaa763

Zank, G. P., Rice, W. K. M., and Wu, C. C. (2000). Particle acceleration and coronal mass ejection driven shocks: A theoretical model. *J. Geophys. Res. Space Phys.* 105, 25079–25095. doi:10.1029/1999JA000455

Zhang, W. Z., Fu, H. S., Cao, J. B., Liu, Y. Y., Zhao, J. S., Guo, Z. Z., et al. (2022). Draft: A method for wave analyses in space plasmas. *Astrophysical J.* 936, 176. doi:10.3847/1538-4357/ac8872